ISSN 1674-1056
http://cpb.iphy.ac.cn
http://iopscience.iop.org/cpb
中国物理 B
Chinese Physics
中国物理 Chinese Physics B

Acoustic wireless communication based on parameter modulation and complex Lorenz chaotic systems with complex parameters and parametric attractors

Fang-Fang Zhang(张芳芳), Rui Gao(高瑞), and Jian Liu(刘坚)

Citation: Chin. Phys. B, 2021, 30 (**8**): 080503. DOI: 10.1088/1674-1056/ac0905
Journal homepage: http://cpb.iphy.ac.cn; http://iopscience.iop.org/cpb

What follows is a list of articles you may be interested in

Exploring the relationship between fractal features and bacterial essential genes

Yong-Ming Yu(余永明), Li-Cai Yang(杨立才), Qian Zhou(周茜), Lu-Lu Zhao(赵璐璐), Zhi-Ping Liu(刘治平)
Chin. Phys. B, 2016, 25 (**6**): 060503. DOI: 10.1088/1674-1056/25/6/060503

Off-policy integral reinforcement learning optimal tracking control for continuous-time chaotic systems

Wei Qing-Lai, Song Rui-Zhuo, Sun Qiu-Ye, Xiao Wen-Dong
Chin. Phys. B, 2015, 24 (**9**): 090504. DOI: 10.1088/1674-1056/24/9/090504

Structure identification of an uncertain network coupled with complex-variable chaotic systems via adaptive impulsive control

Liu Dan-Feng, Wu Zhao-Yan, Ye Qing-Ling
Chin. Phys. B, 2014, 23 (**4**): 040504. DOI: 10.1088/1674-1056/23/4/040504

Experimental identification of a comb-shaped chaotic region in multiple parameter spaces simulated by the Hindmarsh–Rose neuron model

Jia Bing
Chin. Phys. B, 2014, 23 (**3**): 030505. DOI: 10.1088/1674-1056/23/3/030505

Periodic synchronization of community networks with non-identical nodes uncertain parameters and adaptive coupling strength

Chai Yuan, Chen Li-Qun
Chin. Phys. B, 2014, 23 (**3**): 030504. DOI: 10.1088/1674-1056/23/3/030504

Acoustic wireless communication based on parameter modulation and complex Lorenz chaotic systems with complex parameters and parametric attractors*

Fang-Fang Zhang(张芳芳)[1,2], Rui Gao(高瑞)[1,†], and Jian Liu(刘坚)[3]

[1] *Department of Control Science and Engineering, Shandong University, Jinan* 250061, *China*
[2] *Department of Electrical Engineering and Automation, Qilu University of Technology (Shandong Academy of Sciences), Jinan* 250353, *China*
[3] *School of Mathematical Sciences, University of Jinan, Jinan* 250022, *China*

(Received 12 April 2021; revised manuscript received 26 May 2021; accepted manuscript online 8 June 2021)

As the competition for marine resources is increasingly fierce, the security of underwater acoustic communication has attracted a great deal of attention. The information and location of the communicating platform can be leaked during the traditional underwater acoustic communication technology. According to the unique advantages of chaos communication, we put forward a novel communication scheme using complex parameter modulation and the complex Lorenz system. Firstly, we design a feedback controller and parameter update laws in a complex-variable form with rigorous mathematical proofs (while many previous references on the real-variable form were only special cases in which the imaginary part was zero), which can be realized in practical engineering; then we design a new communication scheme employing parameter modulation. The main parameter spaces of the complex Lorenz system are discussed, then they are adopted in our communication scheme. We also find that there exist parametric attractors in the complex Lorenz system. We make numerical simulations in two channels for digital signals and the simulations verify our conclusions.

Keywords: parameter modulation, identification, chaotic system, acoustic wireless communication

PACS: 05.45.Pq, 05.45.Gg, 05.45.Vx, 05.45.Jn **DOI:** 10.1088/1674-1056/ac0905

1. Introduction

At present, underwater wireless communication network has become the significant object of every maritime country, because it has important theoretical significance and economic value for establishing underwater communication network, underwater wireless navigation, marine environment monitoring, and so on.[1] The design of underwater wireless communication network with high reliability and high security is urgent. The underwater acoustic channel is an open channel, which can be received by hydrophone without encryption protection measures, and the enemy can easily obtain confidential information and threaten our security.

However, the security of underwater wireless communication network is still in its infancy. More and more scholars find the importance of safety issues and gradually carry out the corresponding research. The existing underwater wireless communication security technologies mainly include the following categories: encryption technology, trust technology model, intrusion detection, synchronization and location security, routing security, data fusion security, identity authentication technology and other security technologies.[2–5] Among them, the encryption technology can effectively prevent many attacks such as wiretapping and other attacks.

The chaotic signal, similar to a random signal, has a very complicated trajectory and is difficult to predict. Therefore, it has inherent concealment and is widely used in encryption technology.[6] Its initial value sensitivity and good autocorrelation are conducive to obtain more non-interference chaotic signals, which can be realized by FPGA platform[7] and field programmable analog array (FPAA);[8] the noise-like and low-frequency features lead to the low power consumption, which plays a major role in the underwater devices with limited energy, and makes the chaotic underwater acoustic communication fully developed.

Bai *et al.* presented a new differential chaos shift keying (DCSK) communication system for the underwater acoustic channel.[9] In Ref. [10], a novel energy-saving encryption scheme with chaotic compressive sensing (CCS) was proposed in order to guarantee the security of data. Chen *et al.* put forward a novel multi-carrier chaotic spread-spectrum communication system, which is appropriate for the underwater acoustic communication scenario because of the non-coherent receiver without channel estimation and equalization.[11] However, the above chaotic systems are all chaotic systems in real number domain.

Parameter modulation can hide the information in the parameters of the chaotic system, which is better than other chaos communication technologies and has higher confiden-

*Project supported by the National Natural Science Foundation of China (Grant Nos. U1806202, 61773010, and 61903207), the International Collaborative Research Project of Qilu University of Technology (Grant No. QLUTGJHZ2018020), and Major Scientific and Technological Innovation Projects of Shandong Province, China (Grant Nos. 2019JZZY010731 and 2020CXGC010901).

†Corresponding author. E-mail: gaorui@sdu.edu.cn

© 2021 Chinese Physical Society and IOP Publishing Ltd

tiality. The key of parameter modulation scheme lies in the recovery process of system parameters. Because the parameters of chaotic system are sensitive to the channel environment, it will affect the quality of communication and increase security at the same time.

Adding the information signal to the parameters still needs to ensure that the system is chaotic. This requires the chaotic system to have a good parameter space. After Fowler *et al.*[12] discovered the complex Lorenz system in 1982, the complex Lorenz system has been widely applied to detuned laser, rotating fluids,[13] etc. Many researchers achieved the synchronization of the complex Lorenz system and other complex chaotic systems, and adopted them to develop the encryption technology.[14–16]

From the above discussions, we propose a new communication scheme employing complex parameter modulation and the complex Lorenz system for underwater wireless communication network. We find that there exist large parameter space and parametric attractors in the complex Lorenz system. The main contributions are summarized below:

(1) We design an adaptive feedback controller and parameter updates laws in complex-variable form with rigorous mathematical proofs in complex-variable form while many previous references on real-variable form were only special cases where the imaginary part was zero.

(2) We design a new communication scheme based on complex parameter modulation and the complex Lorenz system, and we can modulate multiple parameters with multiple information signals while the number of channels remains unchanged.

(3) For maintain chaotic characteristics, the main parameter space of the complex Lorenz system and its parametric attractors are analyzed.

(4) We make simulations in two channels for digital signal. The simulations verify our conclusions.

The rest of our paper is arranged as follows: We design an adaptive error feedback controller and parameter update laws in Section 2 and present secure communication scheme for underwater wireless communication network in Section 3. Section 4 is devoted to the main parameter space of the complex Lorenz system. We make simulations in two channels in Section 5. Finally, we sum up the whole paper and give some conclusions in Section 6.

2. Adaptive controller and parameters identification

2.1. The design of adaptive controller

We adopt the following CVCS as the response system,

$$\dot{\boldsymbol{x}} = \boldsymbol{F}(x)\boldsymbol{A} + \boldsymbol{f}(\boldsymbol{x}) + \boldsymbol{v} + \boldsymbol{d}_1, \tag{1}$$

where $\boldsymbol{x} = (x_1, x_2, \ldots, x_n)^{\mathrm{T}}$ is the complex-variable vector (superscript T indicates transpose); $\boldsymbol{x} = \boldsymbol{x}^{\mathrm{r}} + j\boldsymbol{x}^{\mathrm{i}}$, with $j = \sqrt{-1}$ being the imaginary unit, and superscript r the real part of $\boldsymbol{x}$ while i the imaginary one; $\boldsymbol{f} = (f_1, f_2, \ldots, f_n)^{\mathrm{T}}$ is a state vector composed of complex-variable functions. $\boldsymbol{F}(x)$ is an $n \times m$ matrix, which is composed of complex-variable functions. $\boldsymbol{A} = (a_1, a_2, \ldots, a_m)^{\mathrm{T}}$ is an $m \times 1$ complex (or real) vector of uncertain parameters; $\boldsymbol{d}_1 = (d_{11}, d_{12}, \ldots, d_{1n})^{\mathrm{T}}$ denotes the bounded external disturbance vector; $|\, d_{1l} \,| < \rho_1$ for $l = 1, 2, \ldots, n$, where $|\cdot|$ represents the modulus of one complex number and ρ_1 is one positive real constant.

If $\boldsymbol{A}$ is a complex vector, $\boldsymbol{A}$ can be expressed as $\boldsymbol{A} = \boldsymbol{A}^{\mathrm{r}} + j\boldsymbol{A}^{\mathrm{i}}$. Therefore, the response system (1) becomes

$$\begin{aligned} \dot{\boldsymbol{x}} &= \boldsymbol{F}(x)\boldsymbol{A}^{\mathrm{r}} + \boldsymbol{j}F(x)\boldsymbol{A}^{\mathrm{i}} + \boldsymbol{f}(\boldsymbol{x}) + \boldsymbol{v} + \boldsymbol{d}_1 \\ &= \boldsymbol{F}(x)\boldsymbol{A}^{\mathrm{r}} + \boldsymbol{Q}(x)\boldsymbol{A}^{\mathrm{i}} + \boldsymbol{f}(\boldsymbol{x}) + \boldsymbol{v} + \boldsymbol{d}_1, \end{aligned} \tag{2}$$

where $\boldsymbol{Q}(\boldsymbol{x}) = j\boldsymbol{F}(\boldsymbol{x})$ is a new $n \times m$ matrix with complex-variable state.

We adopt the same CVCS as the drive system,

$$\dot{\boldsymbol{y}} = \boldsymbol{F}(\boldsymbol{y})\boldsymbol{B} + \boldsymbol{f}(\boldsymbol{y}) + \boldsymbol{d}_2, \tag{3}$$

where $\boldsymbol{B} = (b_1, b_2, \ldots, b_m)^{\mathrm{T}}$ is a complex (or real) vector of $m \times 1$ parameters. We can choose some parameters to modulate multiple messages.

Assumption 1 The complex function vector $\boldsymbol{f}$ satisfies local Lipchitz condition, i.e., for any compact set S, there exist positive constants $l_{\mathrm{rmax}}(S)$ and $l_{\mathrm{imax}}(S)$ such that

$$\begin{aligned} \|\boldsymbol{f}(\boldsymbol{x}) - \boldsymbol{f}(\boldsymbol{y})\| &= \|\boldsymbol{f}(\boldsymbol{x})^{\mathrm{r}} - \boldsymbol{f}(\boldsymbol{y})^{\mathrm{r}} + j(\boldsymbol{f}(\boldsymbol{x})^{\mathrm{i}} - \boldsymbol{f}(\boldsymbol{y})^{\mathrm{i}})\| \\ &\le \|\boldsymbol{f}(\boldsymbol{x})^{\mathrm{r}} - \boldsymbol{f}(\boldsymbol{y})^{\mathrm{r}}\| + \|\boldsymbol{f}(\boldsymbol{x})^{\mathrm{i}} - \boldsymbol{f}(\boldsymbol{y})^{\mathrm{i}}\| \\ &\le [l_{\mathrm{rmax}}(S) + l_{\mathrm{imax}}(S)]\|\boldsymbol{x} - \boldsymbol{y}\| \\ &= l_{\mathrm{fmax}}\|\boldsymbol{x} - \boldsymbol{y}\|, \quad \forall x, y \in S, \end{aligned} \tag{4}$$

where $\|\cdot\|$ means the Euclidean norm. The existence of $l_{\mathrm{rmax}}(S)$, $l_{\mathrm{imax}}(S)$ and $l_{\mathrm{fmax}}(S)$ are associated with the compact set S.

Based on the idea of error feedback,[17,18] we set $\boldsymbol{e} = \boldsymbol{x} - \boldsymbol{y}$ and obtain:

Theorem 1 If we devise the following controller:

$$\boldsymbol{v} = -\boldsymbol{K}\boldsymbol{e}, \tag{5}$$

and the adaptive laws

$$\begin{aligned} \frac{\mathrm{d}\Delta\boldsymbol{A}^{\mathrm{r}}}{\mathrm{d}t} &= -\boldsymbol{\eta}[\boldsymbol{F}^{\mathrm{H}}\boldsymbol{e}]^{\mathrm{r}} = \boldsymbol{\eta}[\boldsymbol{F}^{\mathrm{T}}(x)^{\mathrm{r}}, \boldsymbol{F}^{\mathrm{T}}(x)^{\mathrm{i}}] \begin{bmatrix} \boldsymbol{e}^{\mathrm{r}} \\ \boldsymbol{e}^{\mathrm{i}} \end{bmatrix}, \\ \frac{\mathrm{d}\Delta\boldsymbol{A}^{\mathrm{i}}}{\mathrm{d}t} &= -\boldsymbol{\eta}[\boldsymbol{F}^{\mathrm{H}}\boldsymbol{e}]^{\mathrm{i}} = \boldsymbol{\eta}[\boldsymbol{Q}^{\mathrm{T}}(x)^{\mathrm{r}}, \boldsymbol{Q}^{\mathrm{T}}(x)^{\mathrm{i}}] \begin{bmatrix} \boldsymbol{e}^{\mathrm{r}} \\ \boldsymbol{e}^{\mathrm{i}} \end{bmatrix}, \end{aligned} \tag{6}$$

where $\boldsymbol{\eta} = \mathrm{diag}(\eta_1, \eta_2, \ldots, \eta_m)$ is a factor matrix, which is composed of positive real constants. $\boldsymbol{K} = \mathrm{diag}(k_1, k_2, \ldots, k_n)$ is the control strength matrix in real field, $\Delta\boldsymbol{A} = \boldsymbol{A} - \boldsymbol{B}$ is the parameter error between two systems, then there exists an arbitrarily small positive real number δ which satisfies

$\lim_{t\to\infty}\|\boldsymbol{e}(t)\|^2 \le \delta$, i.e., system (2) asymptotically follows the trajectory of system (3) with the error diminishing to an arbitrarily small degree. It denotes that systems (2)–(3) achieve complete synchronization (CS).

Proof From Eqs. (2), (3) and (5), we obtain

$$\begin{aligned}\dot{\boldsymbol{e}} &= \dot{\boldsymbol{x}}-\dot{\boldsymbol{y}}\\ &= \boldsymbol{F}(\boldsymbol{x})\boldsymbol{A}+\boldsymbol{f}(\boldsymbol{x})-\boldsymbol{K}\boldsymbol{e}-\boldsymbol{F}(\boldsymbol{y})\boldsymbol{B}-\boldsymbol{f}(\boldsymbol{y})+\boldsymbol{d}_1-\boldsymbol{d}_2\\ &= \boldsymbol{F}(\boldsymbol{x})\boldsymbol{A}-\boldsymbol{F}(\boldsymbol{x})\boldsymbol{B}+\boldsymbol{F}(\boldsymbol{x})\boldsymbol{B}-\boldsymbol{F}(\boldsymbol{y})\boldsymbol{B}\\ &\quad -\boldsymbol{K}\boldsymbol{e}+\boldsymbol{f}(\boldsymbol{x})-\boldsymbol{f}(\boldsymbol{y})+\Delta\boldsymbol{d}\\ &= \boldsymbol{F}(\boldsymbol{x})\Delta\boldsymbol{A}+[\boldsymbol{F}(\boldsymbol{x})-\boldsymbol{F}(\boldsymbol{y})]\boldsymbol{B}\\ &\quad -\boldsymbol{K}\boldsymbol{e}+\boldsymbol{f}(\boldsymbol{x})-\boldsymbol{f}(\boldsymbol{y})+\Delta\boldsymbol{d},\end{aligned}\tag{7}$$

where $\Delta\boldsymbol{d}=\boldsymbol{d}_1-\boldsymbol{d}_2$ is the difference between interferences $\boldsymbol{d}_1$ and $\boldsymbol{d}_2$ with $\|\Delta\boldsymbol{d}\|\le\sqrt{n}(\rho_1+\rho_2)$.

We choose the nonnegative Lyapunov function as

$$V(e,t)=\boldsymbol{e}^{\mathrm{H}}\boldsymbol{e}+\Delta\boldsymbol{A}^{\mathrm{H}}\boldsymbol{\eta}^{-1}(\Delta\boldsymbol{A}),\tag{8}$$

where H means conjugate transpose. Therefore,

$$\begin{aligned}\dot{V} &= (\dot{\boldsymbol{e}})^{\mathrm{H}}\boldsymbol{e}+\boldsymbol{e}^{\mathrm{H}}(\dot{\boldsymbol{e}})+(\frac{\mathrm{d}\Delta\boldsymbol{A}}{\mathrm{d}t})^{\mathrm{H}}\boldsymbol{\eta}^{-1}(\Delta\boldsymbol{A})+(\Delta\boldsymbol{A})^{\mathrm{H}}\boldsymbol{\eta}^{-1}(\frac{\mathrm{d}\Delta\boldsymbol{A}}{\mathrm{d}t})\\ &= (\boldsymbol{F}(\boldsymbol{x})\Delta\boldsymbol{A}+[\boldsymbol{F}(\boldsymbol{x})-\boldsymbol{F}(\boldsymbol{y})]\boldsymbol{B}\\ &\quad -\boldsymbol{K}\boldsymbol{e}+\boldsymbol{f}(\boldsymbol{x})-\boldsymbol{f}(\boldsymbol{y})+\Delta\boldsymbol{d})^{\mathrm{H}}\boldsymbol{e}\\ &\quad +\boldsymbol{e}^{\mathrm{H}}(\boldsymbol{F}(\boldsymbol{x})\Delta\boldsymbol{A}+[\boldsymbol{F}(\boldsymbol{x})-\boldsymbol{F}(\boldsymbol{y})]\boldsymbol{B}\\ &\quad -\boldsymbol{K}\boldsymbol{e}+\boldsymbol{f}(\boldsymbol{x})-\boldsymbol{f}(\boldsymbol{y})+\Delta\boldsymbol{d})\\ &\quad -\boldsymbol{\eta}(\boldsymbol{F}^{\mathrm{H}}\boldsymbol{e})^{\mathrm{H}}\boldsymbol{\eta}^{-1}(\Delta\boldsymbol{A})-\Delta\boldsymbol{A}^{\mathrm{H}}\boldsymbol{\eta}^{-1}\boldsymbol{\eta}(\boldsymbol{F}^{\mathrm{H}}\boldsymbol{e})\\ &= ([\boldsymbol{F}(\boldsymbol{x})-\boldsymbol{F}(\boldsymbol{y})]\boldsymbol{B}-\boldsymbol{K}\boldsymbol{e}+\boldsymbol{f}(\boldsymbol{x})-\boldsymbol{f}(\boldsymbol{y})+\Delta\boldsymbol{d})^{\mathrm{H}}\boldsymbol{e}\\ &\quad +\boldsymbol{e}^{\mathrm{H}}([\boldsymbol{F}(\boldsymbol{x})-\boldsymbol{F}(\boldsymbol{y})]\boldsymbol{B}-\boldsymbol{K}\boldsymbol{e}+\boldsymbol{f}(\boldsymbol{x})-\boldsymbol{f}(\boldsymbol{y})+\Delta\boldsymbol{d}).\end{aligned}\tag{9}$$

where the over dot means the derivative with respect time t. According to Assumption 1, we assume that there exist an $n\times n$ $l_{\mathrm{Fmax}}(t)$ satisfying $||[\boldsymbol{F}(\boldsymbol{x})-\boldsymbol{F}(\boldsymbol{y})]\boldsymbol{B}||\le l_{\mathrm{Fmax}}(t)||\boldsymbol{x}-\boldsymbol{y}||$ and an $n\times n$ $l_{\mathrm{fmax}}(t)$ satisfying $||\boldsymbol{f}(\boldsymbol{x})-\boldsymbol{f}(\boldsymbol{y})||\le l_{\mathrm{fmax}}(t)||\boldsymbol{x}-\boldsymbol{y}||$. Then we obtain

$$\begin{aligned}\dot{V} &\le \boldsymbol{e}^{\mathrm{H}}[l_{\mathrm{Fmax}}^{\mathrm{H}}+l_{\mathrm{Fmax}}+l_{\mathrm{fmax}}^{\mathrm{H}}+l_{\mathrm{fmax}}-\boldsymbol{K}^{\mathrm{H}}-\boldsymbol{K}]\boldsymbol{e}\\ &\quad +\boldsymbol{e}^{\mathrm{H}}\Delta\boldsymbol{d}+\Delta\boldsymbol{d}^{\mathrm{H}}\boldsymbol{e}.\end{aligned}\tag{10}$$

As $\boldsymbol{K}$ is the diagonal matrix and its elements are arbitrarily large positive in Eq. (10), we select a suitable $\boldsymbol{K}$ satisfying $\{l_{\mathrm{Fmax}}^{\mathrm{H}}+l_{\mathrm{Fmax}}+l_{\mathrm{fmax}}^{\mathrm{H}}+l_{\mathrm{fmax}}-\boldsymbol{K}^{\mathrm{H}}-\boldsymbol{K}\}$ negative definite matrix, and $-L(L>0)$ is its maximum eigenvalue.

We set $\|\boldsymbol{e}\|^2=\delta$, and obtain

$$\begin{aligned}\boldsymbol{e}^{\mathrm{H}}\Delta\boldsymbol{d}+\Delta\boldsymbol{d}^{\mathrm{H}}\boldsymbol{e} &\le \|\boldsymbol{e}\|\sqrt{n}(\rho_1+\rho_2)+\sqrt{n}(\rho_1+\rho_2)\|\boldsymbol{e}\|\\ &= \sqrt{n\delta}(\rho_1+\rho_2)\\ &< C\delta,\end{aligned}\tag{11}$$

where C is a positive constant in the real field and $C>\sqrt{n/\delta}(\rho_1+\rho_2)$.

We select a suitable $\boldsymbol{K}$ to ensure $L>C$. Therefore, we get $\dot{V}\le -L\|\boldsymbol{e}\|^2+C\delta\le -(L-C)\delta<0$. Hence, system (2) asymptotically follows the trajectory of system (3) with an arbitrarily small error. The proof is finished.

In addition, from Eq. (6), $\boldsymbol{A}$ tends to a constant vector when $\boldsymbol{e}\to 0$. We will discuss the astringency of unknown parameters in the following section.

Remark 1 We can rewrite Eq. (6) into $\frac{\mathrm{d}\Delta\boldsymbol{A}}{\mathrm{d}t}=-\boldsymbol{\eta}[\boldsymbol{F}^{\mathrm{H}}\boldsymbol{e}]$. It indicates that Theorem 1 really generalizes a chaotic system and its parameter identification into the complex-variable field.

2.2. Astringency of unknown parameters

The identification and astringency of unknown parameters depend on conditions of complex linear independence (CLI) which we discuss in this section.

Lemma 1 (CLI)[19,20] The set of complex-variable function $\{\omega_k(x),k=1,2,\ldots,n\}$ is called complex linear independence in the set Γ if and only if

$$\sum_{k=1}^{n}d_k[\omega_k(x)^{\mathrm{r}}+j\omega_k(x)^{\mathrm{i}}]=0,\quad \forall x\in\Gamma,d_k\in C\tag{12}$$

under the condition $d_k=0,k=1,2,\ldots,n$.

However, if $\{\omega_k(x)^{\mathrm{r}},k=1,2,\ldots,n\}$ or $\{\omega_k(x)^{\mathrm{i}},k=1,2,\ldots,n\}$ is linearly independent, then complex-variable function $\{\omega_k(x),k=1,2,\ldots,n\}$ is not definitely complex linearly independent. For example, $\{c_1+c_2j,c_2-c_1j\}$ is not complex linear independence (because $c_1+c_2j=j(c_2-c_1j)$) although $\{c_1+c_2j,c_2-c_1j\}$ is real linear independence[20] in real field.

When we discuss the astringency conditions in the complex field, we neglect the influence of interferences, because the interferences are bounded with small amplitude.

From Eq. (7), we have

$$\begin{aligned}\dot{\boldsymbol{e}} &= \boldsymbol{F}(\boldsymbol{x})\Delta\boldsymbol{A}+[\boldsymbol{F}(\boldsymbol{x})-\boldsymbol{F}(\boldsymbol{y})]\boldsymbol{B}\\ &\quad -\boldsymbol{K}\boldsymbol{e}+\boldsymbol{f}(\boldsymbol{x})-\boldsymbol{f}(\boldsymbol{y}).\end{aligned}\tag{13}$$

From Theorem 1, we obtain $\dot{\boldsymbol{e}}\to 0$ and $\boldsymbol{x}\to\boldsymbol{y}$. Hence,

$$\boldsymbol{F}(\boldsymbol{x})\Delta\boldsymbol{A}=\boldsymbol{F}(\boldsymbol{x})(\boldsymbol{A}-\boldsymbol{B})\to 0.\tag{14}$$

According to CLI, the sufficient condition of $\boldsymbol{A}-\boldsymbol{B}\to 0$ is that complex-variable function set $\{\boldsymbol{F}(\boldsymbol{x})\}$ is complex linear independence.

3. Acoustic secure communication schemes based on parameter modulation

3.1. Acoustic secure communication schemes

Here we propose an acoustic secure communication scheme based on parameter modulation. The diagram of the presented communication scheme is shown in Fig. 1. The electrical signal $\boldsymbol{y}$, produced by the driver system at the sender end

(which can be realized by FPGA in practice), is converted to acoustic signal and transmitted to the receiver. The response system represents the receiver. It receives acoustic signal and converts it to the electrical signal. The information signal or plaintext is $\boldsymbol{m}(t)$, the recovered information signal is $\boldsymbol{m}'(t)$, and D is the proportional matrix. The actual parameter at the sender $\boldsymbol{B} = \boldsymbol{B}_{\text{ref}} + \boldsymbol{D}\boldsymbol{m}(t)$.

For a practical underwater wireless communication scheme, the sender presents the underwater node which collects useful information and needs to be encrypted, while the receiver indicates underwater sink node. It also represents the process that the underwater sink node (the sender end) processes the data and transmits it to the surface base station or gateway node (the receiver end) through the vertical communication link.

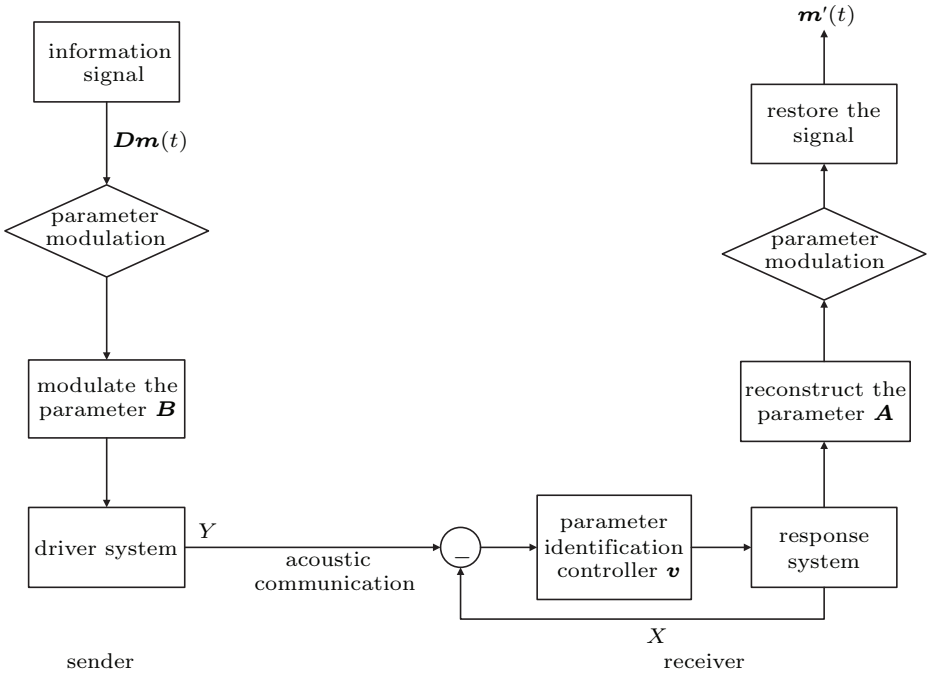


Fig. 1. The diagram of communication scheme based on parameter modulation.

We take into account the noise in the communication channel, and obtain the actual transmitted signal

$$\boldsymbol{s}(t) = \boldsymbol{y}(t) + \boldsymbol{P}\boldsymbol{\varepsilon}(t), \tag{15}$$

where $\boldsymbol{P}\boldsymbol{\varepsilon}(t)$ represents the noise in a given channel generated by all noise sources and $\boldsymbol{P}$ denotes the amplitude of the noise.

The communication process is divided into two parts. First, the initial value of the sender $\boldsymbol{y}(0)$ is broadcasted to the receiver. For starting communication, $\boldsymbol{y}(0)$ is applied to provide the receiver with a command to begin sending the transmitted signal. In the second part, after receiving the correctly returned signal $\boldsymbol{y}(0)$ from the receiver, the sender begins to produce the transmitted signal $\boldsymbol{s}(t)$ produced by actual parameter $\boldsymbol{B}$, which conceals the message signal $\boldsymbol{m}(t)$.

The encryption method of the sender end consists of both chaotic-parameter encryption and noise-masking technology. At the receiving end, the controller $\boldsymbol{v}$ and parameter identification schemes are designed in Theorem 1 which includes $\boldsymbol{y} = \boldsymbol{s} - P\boldsymbol{\varepsilon}(t)$ (we filter $\boldsymbol{s}$ and obtain the effective transmitted signal $\boldsymbol{y}$. The filter can be realized by various filtering methods, such as mean filtering, median filtering and boundary preserving filtering. Here we adopt mean filtering). As CS is achieved, the parameter vector in the response system is $\boldsymbol{A} = \boldsymbol{B} = \boldsymbol{B}_{\text{ref}} + \boldsymbol{D}\boldsymbol{m}(t)$. Therefore, the recovered signal is $\boldsymbol{m}'(t) = \boldsymbol{D}^{-1}(\boldsymbol{A} - \boldsymbol{B}_{\text{ref}})$.

Moreover, the driver system with the actual parameter range of $\boldsymbol{B} = \boldsymbol{B}_{\text{ref}} + \boldsymbol{D}\boldsymbol{m}(t)$ should be chaotic. Here, we choose the complex Lorenz system as driver-response systems. Therefore, we need to search the parameter space of the complex Lorenz system.

3.2. The parameter space of the complex Lorenz system with complex parameter

The complex Lorenz system with complex parameters usually has large parameter space. We will analyze the parameter range of maintaining the system chaotic.

The complex Lorenz system[12,21,22] is as follows:

$$\begin{aligned} \dot{y}_1 &= b_1(y_2 - y_1), \\ \dot{y}_2 &= b_2 y_1 - b_3 y_2 - y_1 y_3, \\ \dot{y}_3 &= -b_4 y_3 + (1/2)(\bar{y}_1 y_2 + y_1 \bar{y}_2). \end{aligned} \tag{16}$$

where y_1, y_2 are state variables in complex field while y_3 is a state variable in real field. $\boldsymbol{B} = (b_1, b_2, b_3, b_4)^{\mathrm{T}}$ is the complex parameter vector.

The initial points are $\boldsymbol{y}(0) = (1+2j, 3+4j, 5)^{\mathrm{T}}$. The fourth-order Runge-Kutta scheme in complex-variable field is utilized to solve the differential equations with $\Delta t = 10^{-3}$. When $\boldsymbol{B} = (2, 60+0.02j, 1-0.06j, 0.8)^{\mathrm{T}}$, the phase portraits of the complex Lorenz system with complex parameters are demonstrated in Fig. 2.

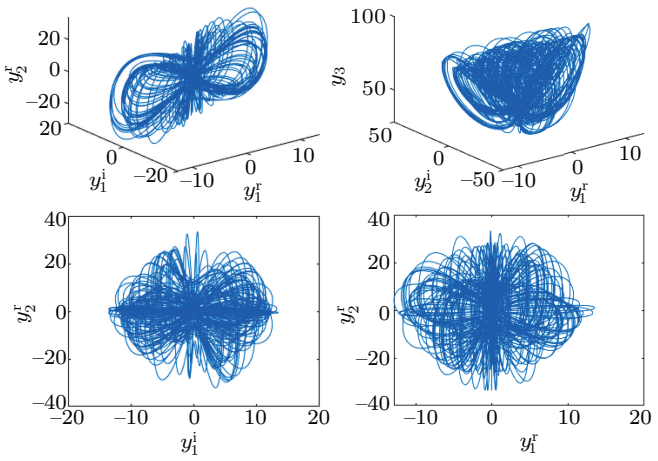


Fig. 2. The attractor of Lorenz system with complex parameters.

(1) Firstly, we get the Lyapunov exponents curve as b_1 changes in Fig. 3. It can be seen that the chaotic space of b_1 is $[2,17]\cup[82,85]$.

We choose some special values of b_1 and get the Lyapunov exponents.

When $b_1 = 1$ (Fig. 4(a)), the Lyapunov exponents are (0, −0.38076, −0.41321, −2.00421, −2.00582). There is no positive Lyapunov exponent, which means limit cycle.

When $b_1 = 2$ (Fig. 2), the Lyapunov exponents are (0.28349, 0, 0, −3.00523, −4.08825). There is one positive Lyapunov exponent, which means chaos.

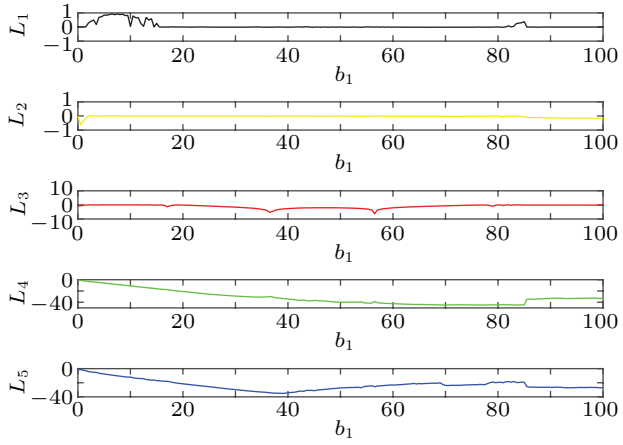


Fig. 3. The Lyapunov exponents curve as b_1 changes.

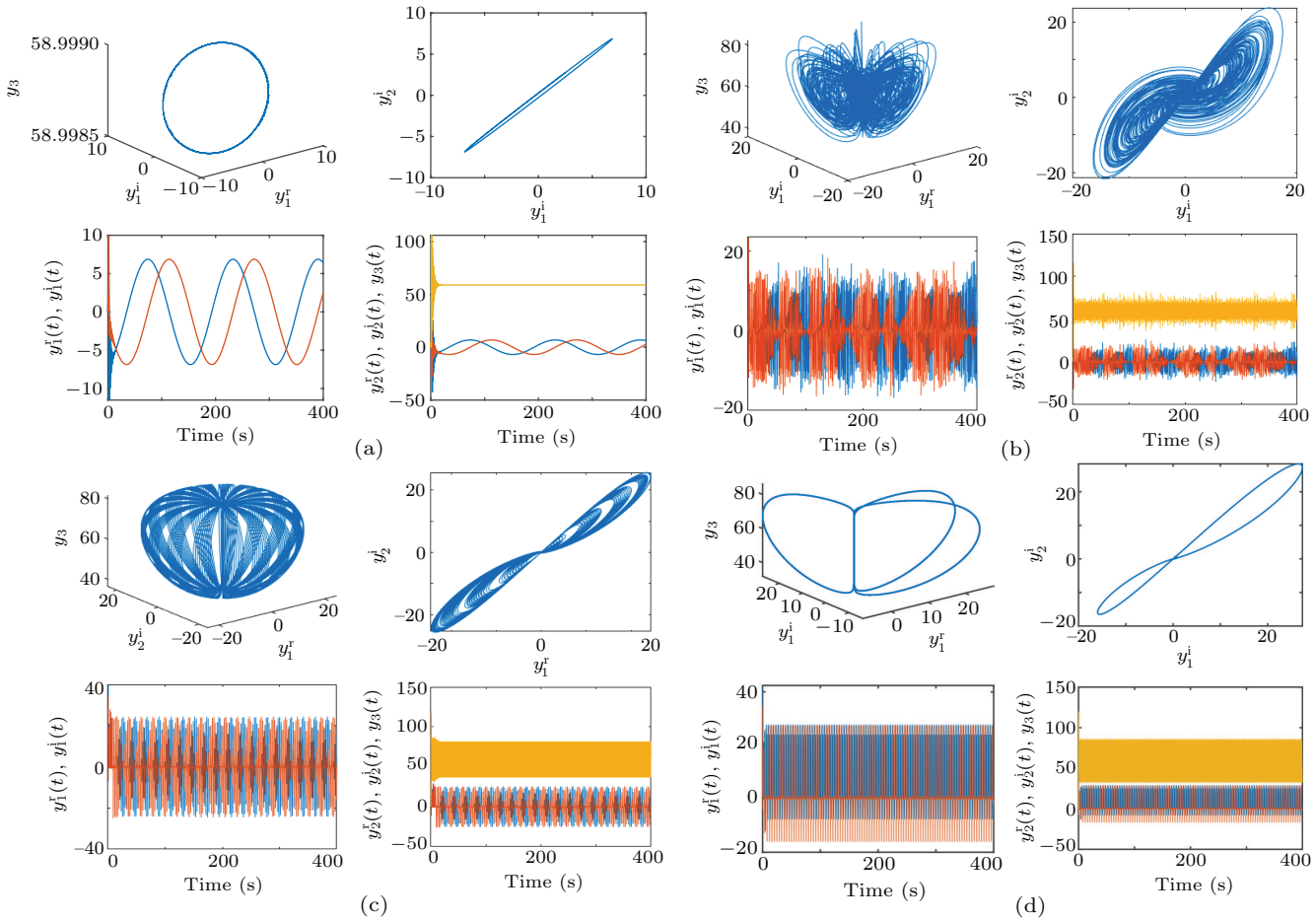


Fig. 4. The phase portraits of the complex Lorenz system for different b_1: (a) $b_1 = 1$, (b) $b_1 = 10$, (c) $b_1 = 60$, (d) $b_1 = 86$.

When $b_1 = 10$ (Fig. 4(b)) the Lyapunov exponents are (0.04841, 0, −0.02380, −10.99931, −11.82599) and it means chaos.

When $b_1 = 60$ (Fig. 4(c)), the Lyapunov exponents are (0, 0, −2.07982, −42.41002, −23.20592). There are two zero Lyapunov exponents and there is no positive exponent. This shows the quasi periodic phenomenon.

When $b_1 = 86$ (Fig. 4(d)), the Lyapunov exponents are (0, −0.12169, −0.14365, −34.09214, −26.29621). It shows limit cycle.

The phase portraits and state variables curve of the complex Lorenz system are shown in Fig. 4. It can be seen that it is not chaotic when $b_1 < 2$, and the Lyapunov exponents are all less than zero; when $2 \leq b_1 \leq 17$, the maximum Lyapunov exponent L1 is the positive real number. When $17 < b_1 < 82$, the state of the complex Lorenz system is periodic or limit cycles. When $82 \leq b_1 \leq 85$, the complex Lorenz system becomes chaotic again.

(2) Secondly, we get the Lyapunov exponents curve as b_2^{r} changes in Fig. 5. It can be seen that the chaotic space of b_2^{r} is $[30, 70]$.

When $b_2^{\mathrm{r}} = 25$ (Fig. 6(a)), the Lyapunov exponents are (0, −0.07349, −0.08246, −3.00038, −3.64533), which means limit cycle.

When $b_2^{\mathrm{r}} = 30$ (Fig. 6(b)), the Lyapunov exponents are (0.37313, 0, −0.01364, −2.99447, −4.16747), which means chaos.

When $b_2^{\mathrm{r}} = 50$ (Fig. 6(c)), the Lyapunov exponents are (0.38532, 0, 0, −3.00426, −4.18414), which means chaos.

When $b_2^{\mathrm{r}} = 80$ (Fig. 6(d)), the Lyapunov exponents are (0.01119, 0, −0.82714, −2.97168, −3.02015), which means chaos.

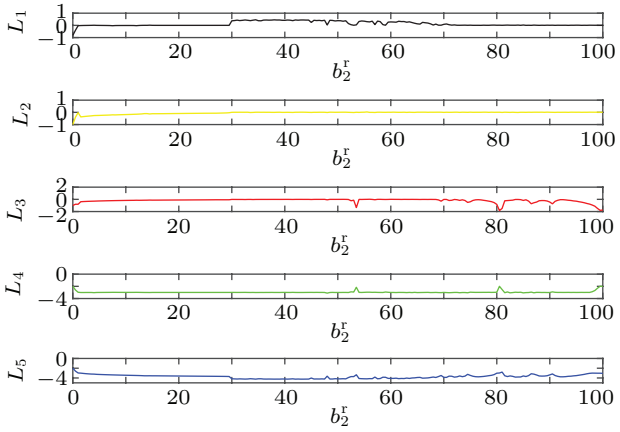


Fig. 5. The Lyapunov exponents versus b_2^{r}.

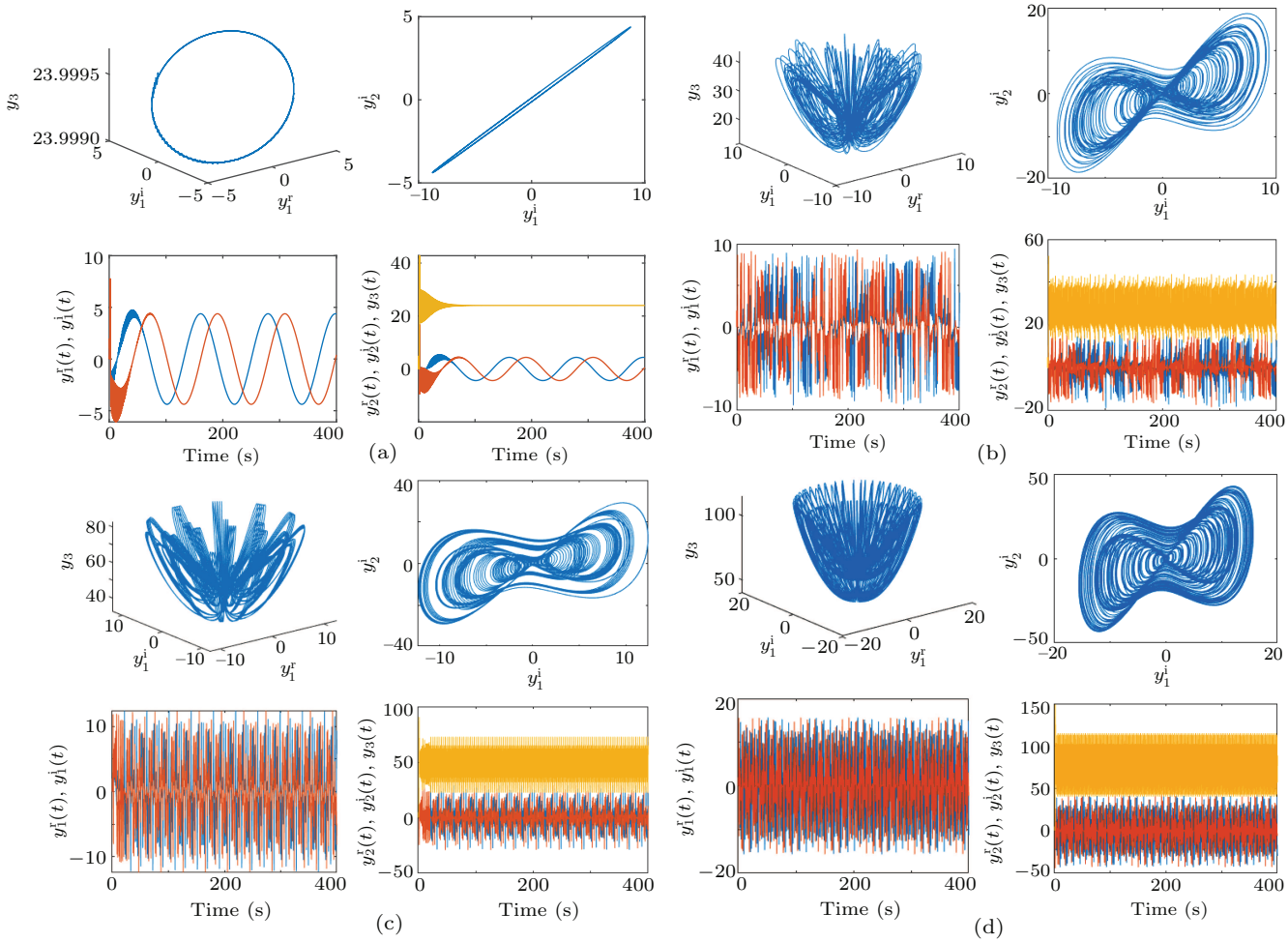


Fig. 6. The phase portraits of the complex Lorenz system for different b_2^{r}: (a) $b_2^{\mathrm{r}} = 25$, (b) $b_2^{\mathrm{r}} = 30$, (c) $b_2^{\mathrm{r}} = 50$, (d) $b_2^{\mathrm{r}} = 80$.

Moreover, there are similar but different attractors when $b_2^{\mathrm{r}} = 30$, $b_2^{\mathrm{r}} = 50$, $b_2^{\mathrm{r}} = 60$ (shown in Fig. 2) and $b_2^{\mathrm{r}} = 80$, and we call them parametric attractors, which are caused by the change of parameters. It is different from coexisting attractors that the initial points are unfixed and all parameters are fixed. Parametric attractors are caused by the change of parameters, while coexisting attractors are produced by the choice of initial points. As the dynamics from parameter domain to the domain of the initial conditions, there are some similarities and symmetry in parametric attractors and coexisting attractors. Besides the complex Lorenz system, some complex chaotic systems also exhibit parametric attractors such as complex Chen system and complex Lü system. For more information, the readers can see Ref. [23].

(3) Thirdly, we get the Lyapunov exponents versus b_2^{i} in Fig. 7. It can be seen that the chaotic space of b_2^{i} is $[-0.1, 0.1]$.

When $b_2^{\mathrm{i}} = -0.8$ (Fig. 8(a)), the Lyapunov exponents are (0, −0.03336, −0.04839, −3.30588, −3.41867), which means limit cycle.

When $b_2^{\mathrm{i}} = 0$ (Fig. 8(b)), the Lyapunov exponents are (0.39006, 0, −0.01275, −3.00225, −4.18334), which means chaos.

When $b_2^{\mathrm{i}} = 0.1$ (Fig. 8(c)), the Lyapunov exponents are (0.19398, 0.01446, 0, −3.01151, −3.99200), which means hyperchaos.

When $b_2^{\mathrm{i}} = 1$ (Fig. 8(d)), the Lyapunov exponents are (0, −0.06426, −0.09835, −3.32354, −3.31866), which means limit cycle.

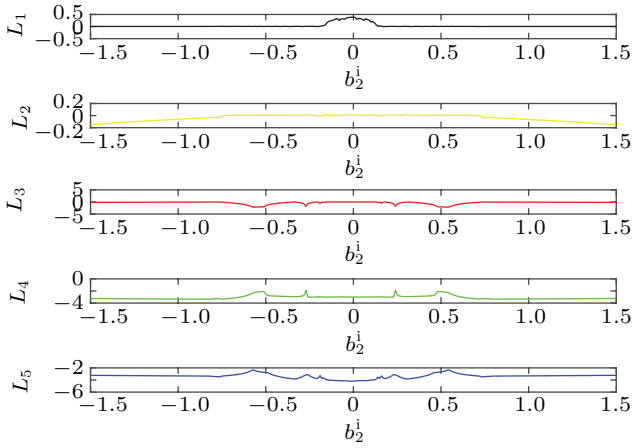


Fig. 7. The Lyapunov exponents versus b_2^{i}.

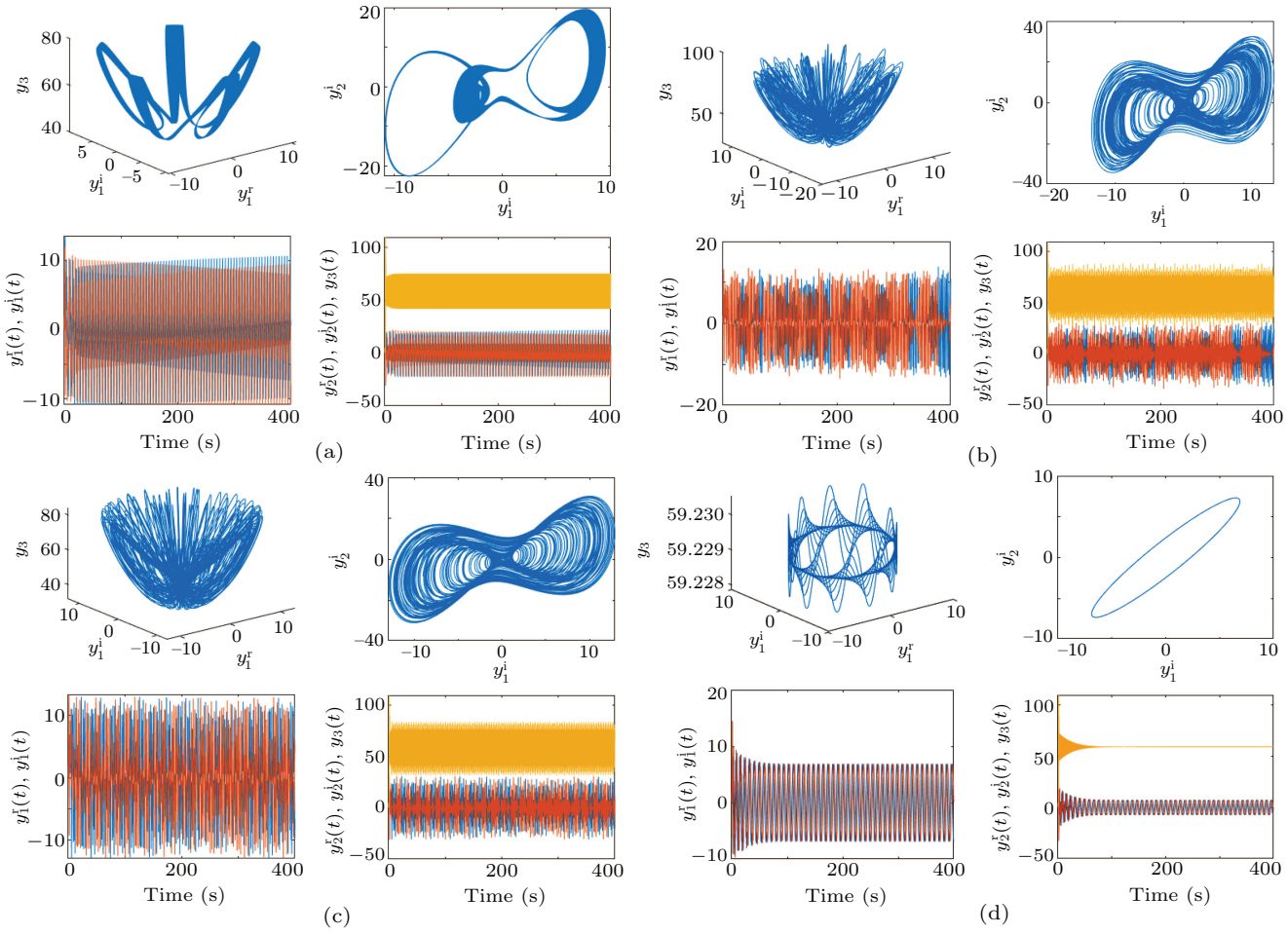


Fig. 8. The phase portraits of the complex Lorenz system for different b_2^{i}: (a) $b_2^{\mathrm{i}} = -0.8$, (b) $b_2^{\mathrm{i}} = 0$, (c) $b_2^{\mathrm{i}} = 0.1$, (d) $b_2^{\mathrm{i}} = 1$.

(4) Fourthly, we get the Lyapunov exponents curve as b_3^{r} changes in Fig. 9. It can be seen that the chaotic space of b_3^{r} is $[-0.9, 1.3]$.

When $b_3^{\mathrm{r}} = 0.1$ (Fig. 10(a)), the Lyapunov exponents are (0, 0, −0.89030, −2.02607, −2.09165), which means quasi-periodic.

When $b_3^{\mathrm{r}} = 0.95$ (Fig. 10(b)), the Lyapunov exponents are (0.25893, 0, 0, −2.94038, −4.00520), which means chaos.

When $b_3^{\mathrm{r}} = 1.2$ (Fig. 10(c)), the Lyapunov exponents are (0.50169, 0.01004, 0, −3.20395, −4.50166), which means hyperchaos.

When $b_3^{\mathrm{r}} = 1.4$ (Fig. 10(d)), the Lyapunov exponents are (0, −0.13193, −0.16684, −3.40533, −3.90376), which means limit cycle.

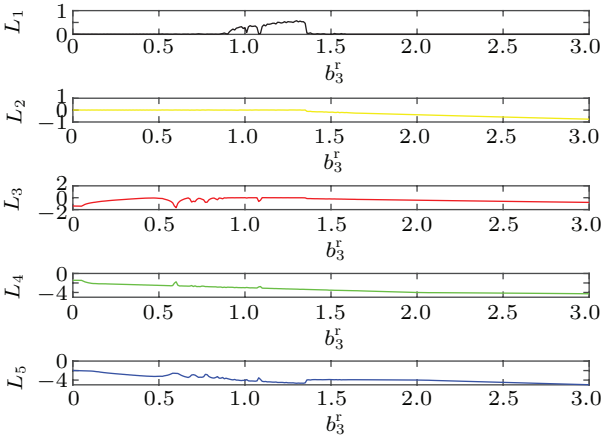


Fig. 9. The Lyapunov exponents versus b_3^{r}.

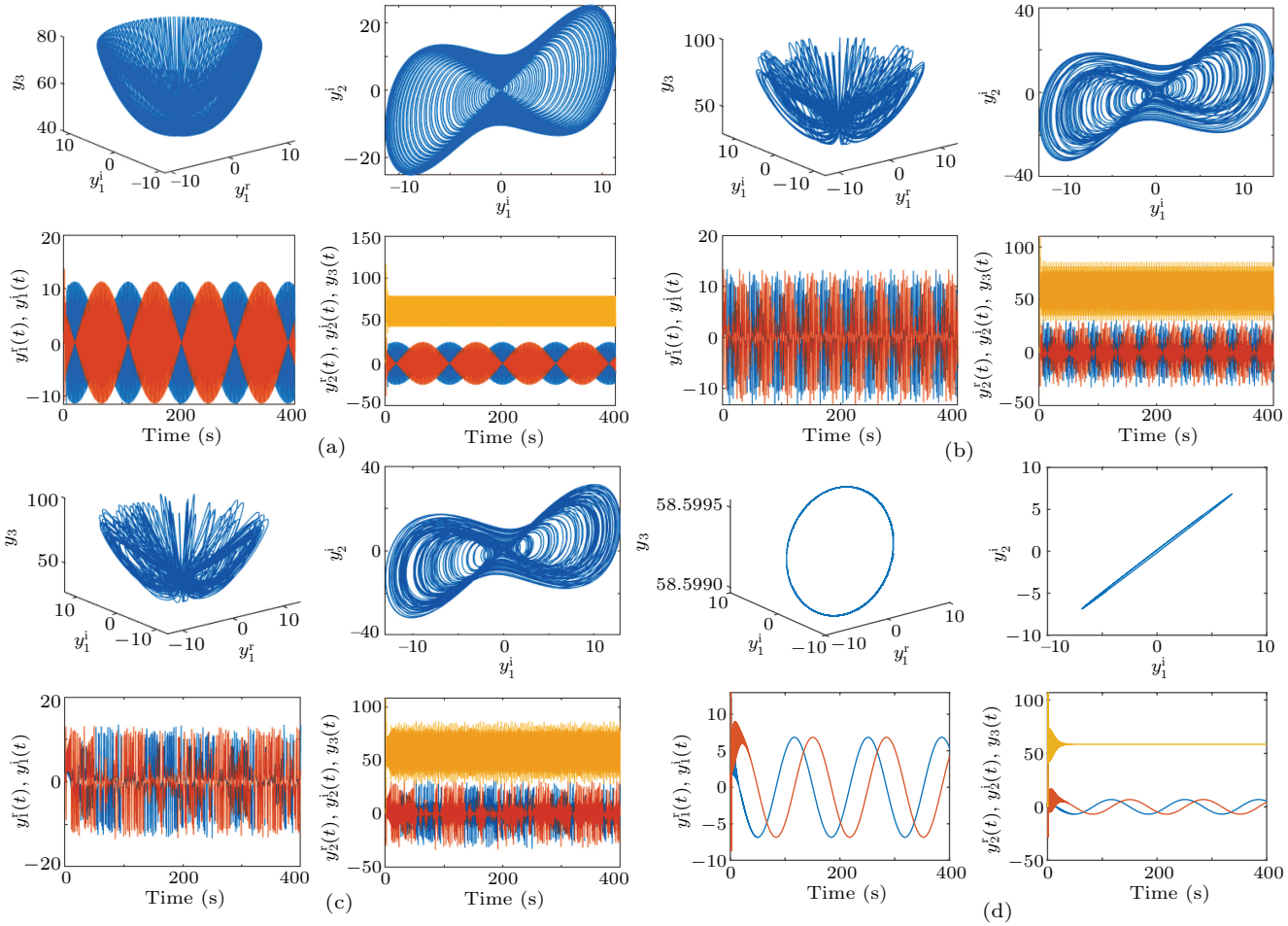


Fig. 10. The phase portraits of the complex Lorenz system for different b_3^{r}: (a) $b_3^{\mathrm{r}} = 0.1$, (b) $b_3^{\mathrm{r}} = 0.95$, (c) $b_3^{\mathrm{r}} = 1.2$, (d) $b_3^{\mathrm{r}} = 1.4$.

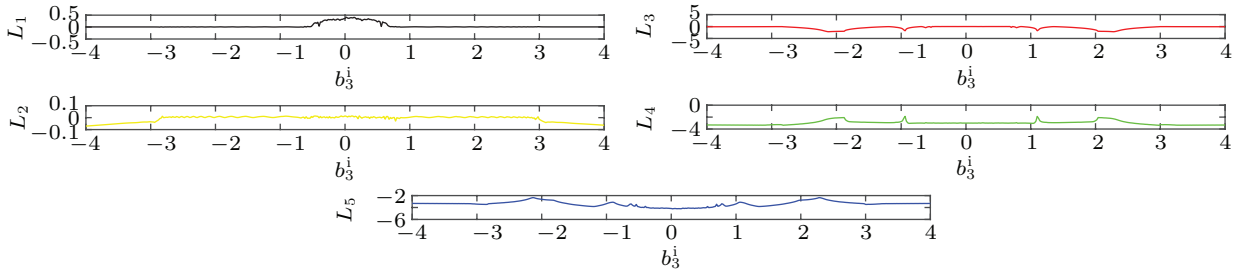


Fig. 11. The Lyapunov exponents versus b_3^{i}.

(5) Fifthly, we get the Lyapunov exponents versus $b_3^{\rm i}$ in Fig. 11. It can be seen that the chaotic space of $b_3^{\rm i}$ is $[-0.5, 0.5]$.

When $b_3^{\rm i} = -4$ (Fig. 12(a)), the Lyapunov exponents are (0, −0.07091, −0.10108, −3.31907, −3.31523), which means limit cycle.

When $b_3^{\rm i} = -3$ (Fig. 12(b)), the Lyapunov exponents are (0, −0.03455, −0.05073, −3.28581, −3.43413), which means limit cycle.

When $b_3^{\rm i} = 0$ (Fig. 12(c)), the Lyapunov exponents are (0.36096, 0.01437, 0, −3.00828, −4.16512), which means hyperchaos.

When $b_3^{\rm i} = 2$ (Fig. 12(d)), the Lyapunov exponents are (0, 0, −1.43586, −2.60664, −2.76792), which means quasi-periodic.

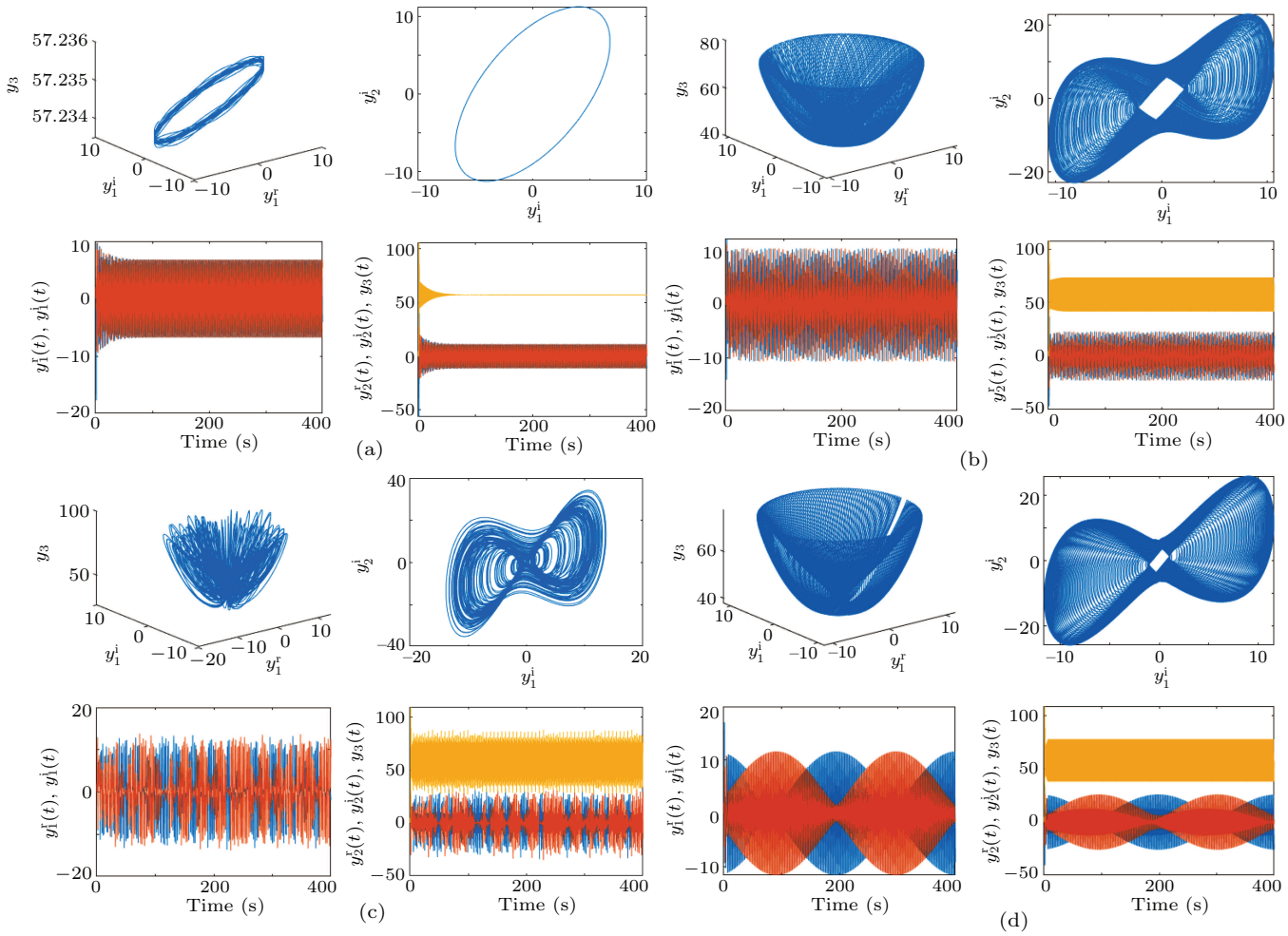


Fig. 12. The phase portraits of the complex Lorenz system for different $b_3^{\rm i}$: (a) $b_3^{\rm i} = -4$, (b) $b_3^{\rm i} = -3$, (c) $b_3^{\rm i} = 0$, (d) $b_3^{\rm i} = 2$.

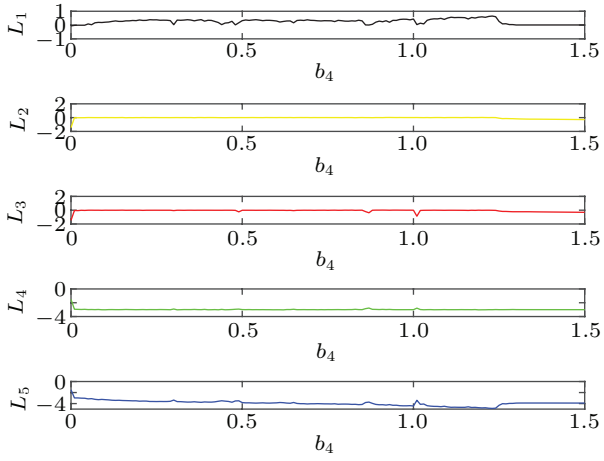


Fig. 13. The Lyapunov exponents versus b_4.

(6) Sixthly, we get the Lyapunov exponents versus b_4 as shown in Fig. 13. It can be seen that the chaotic space of b_4 is $[0.1, 1.3]$.

When $b_4 = 0.01$ (Fig. 14(a)), the Lyapunov exponents are (−0.02278, −0.02196, −0.04565, −2.94407, −2.97556), which means the convergence to one fixed point.

When $b_4 = 0.1$ (Fig. 14(b)), the Lyapunov exponents are (0.20761, 0, −0.00441, −3.01881, −3.29024), which means chaos.

When $b_4 = 1$ (Fig. 14(c)), the Lyapunov exponents are (0.43993, 0, 0, −3.00687, −4.43542), which means chaos.

When $b_4 = 1.4$ (Fig. 14(d)), the Lyapunov exponents are (0, −0.24059, −0.26410, −3.00234, −3.89929), which means limit cycle.

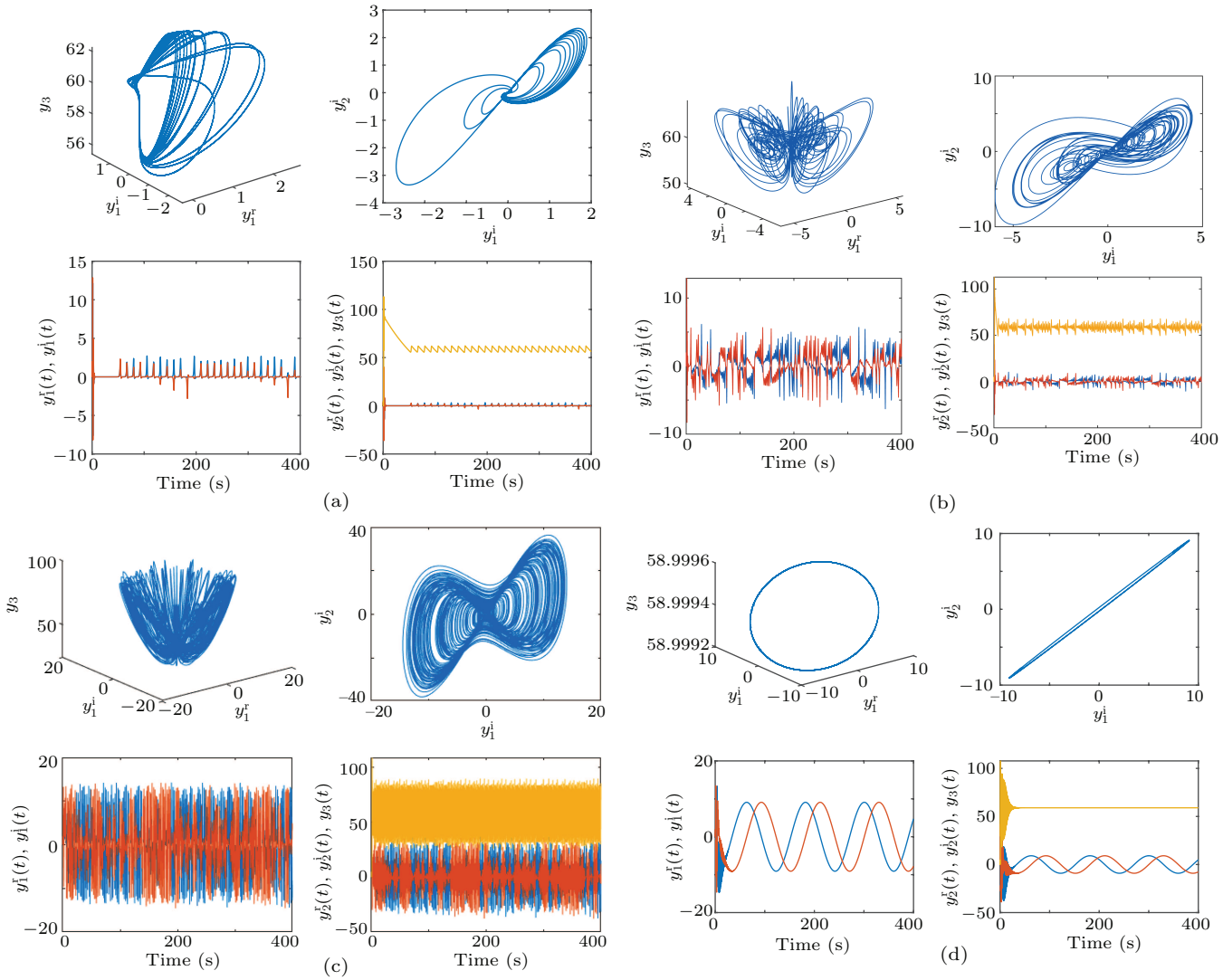


Fig. 14. The phase portraits of the complex Lorenz system for different b_4: (a) $b_4 = 0.01$, (b) $b_4 = 0.1$, (c) $b_4 = 1$, (d) $b_4 = 1.4$.

It also provides a general method to find the parameters space of chaotic system. Here, we select b_1 and b_2^{r} which possess large parameter space to modulate useful message.

4. Numerical simulations

We select $\hat{A}(0) = (1, 1, 1)^{\mathrm{T}}$ as the initial value of uncertain parameter vector in the response system. $\boldsymbol{B}_{\mathrm{ref}}$ is known, and $\boldsymbol{B}_{\mathrm{ref}} = (2, 60 + 0.02j, 1 - 0.06j, 0.8)^{\mathrm{T}}$. We choose $\boldsymbol{K} = \mathrm{diag}(0.1, 0.1, 0.1)^{\mathrm{T}}$ as their control strength, and $\boldsymbol{x}(0) = \boldsymbol{y}(0) = (1 + 2j, 3 + 4j, 5)^{\mathrm{T}}$ as the initial points. The external disturbances are denoted as $d_{11} = \sin(0.5\pi t) + j\cos(\pi t)$, $d_{12} = 0.3\sin(\pi t) + j\cos(\pi t)$, $d_{13} = \sin(0.25\pi t)$, $d_{21} = 0.5\sin(\pi t) + j2\cos(\pi t)$, $d_{22} = 0.3\sin(\pi t) + j0.5\cos(\pi t)$ and $d_{23} = \sin(0.5\pi t)$, and we get $\rho_1 = 1.414$ and $\rho_2 = 2.062$. The random noise with the amplitude $[-10, 10]$ ($P = 10$) in three channels is also considered in simulations. We realize the process of information transmission by Matlab software.

We plan the controller on the basis of Theorem 1,

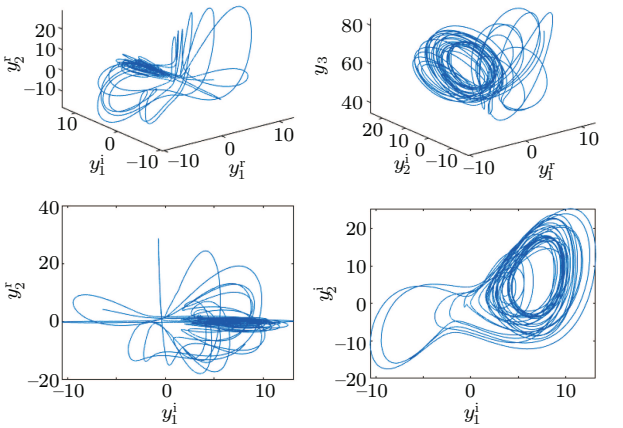


Fig. 15. The phase portraits of the complex Lorenz system when parameter with digital signals.

$$\boldsymbol{v} = -\boldsymbol{K}\boldsymbol{e} = \begin{pmatrix} k_1(x_1 - y_1) \\ k_2(x_2 - y_2) \\ k_3(x_3 - y_3) \end{pmatrix} \tag{17}$$

and the update laws of parameters

$$\dot{\boldsymbol{A}} = \begin{pmatrix} \dot{a}_1 \\ \dot{a}_2^{\mathrm{r}} \end{pmatrix} = \begin{pmatrix} \eta[(x_2 - x_1)^{\mathrm{r}} e_1^{\mathrm{r}} + (x_2 - x_1)^{\mathrm{i}} e_1^{\mathrm{i}}] \\ \eta[x_1^{\mathrm{r}} e_2^{\mathrm{r}} + x_1^{\mathrm{i}} e_2^{\mathrm{i}}] \end{pmatrix}. \tag{18}$$

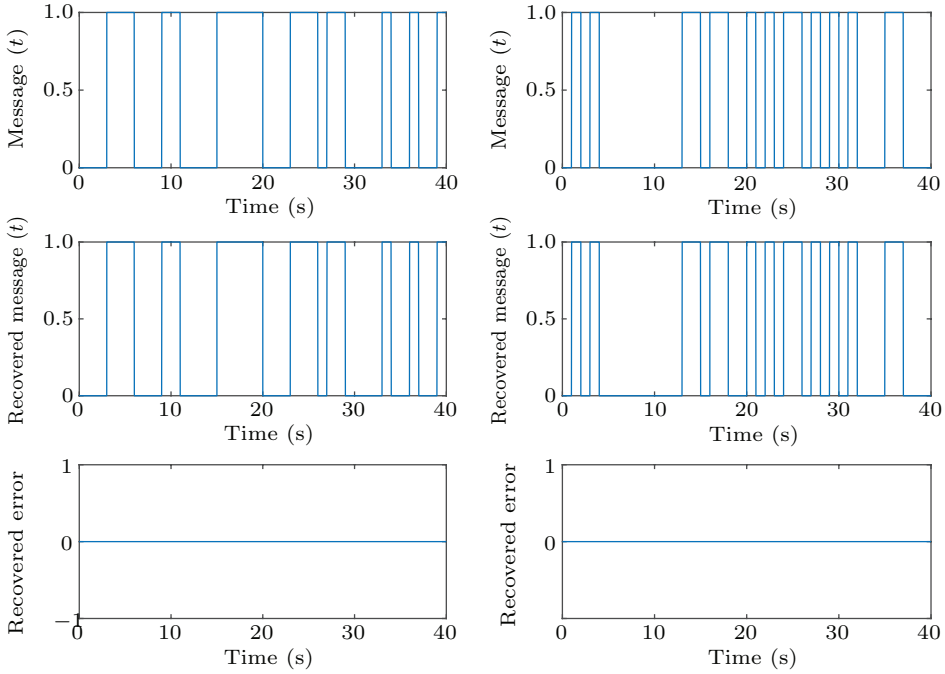


Fig. 16. The message signals and the recovered message signals.

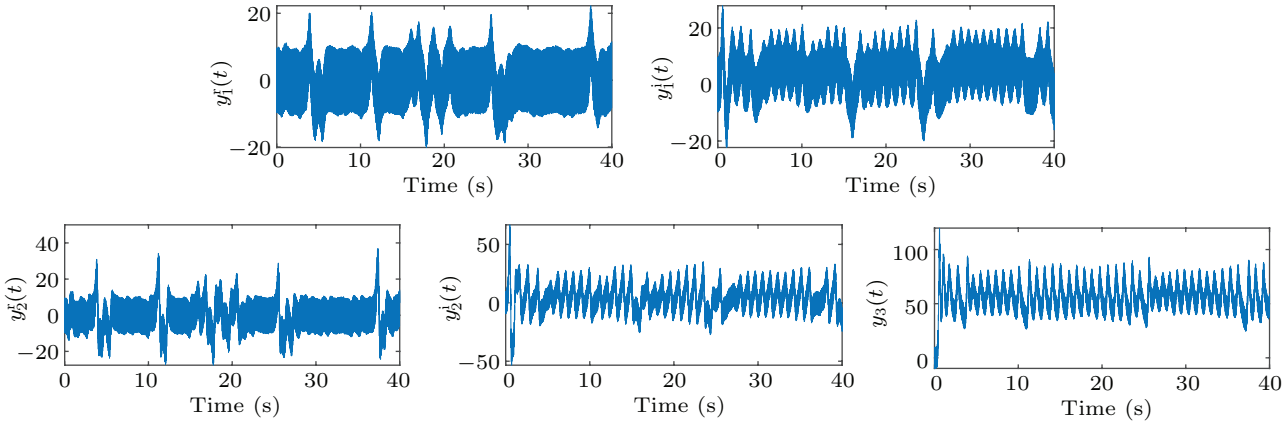


Fig. 17. The transmitted signal $s(t)$ in channels.

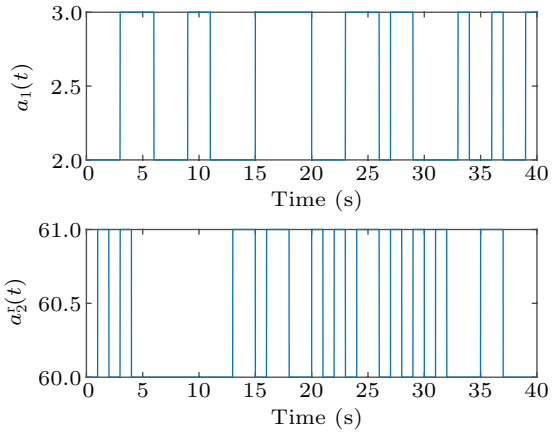


Fig. 18. The identification process of unknown parameter vector $\boldsymbol{A}$.

We adopt b_1 and b_2^{r} to transmit two digital sequences, and the attractor phase portraits of the complex Lorenz system are represented in Fig. 15. It is in chaotic space. The sender collects data during one sampling period. In reality, the marine situation does not change suddenly, the CS controller is available enough in one sampling period. The plaintext message and the recovered message are depicted in Fig. 16, where the plaintext signals are recovered with zero BER (bit error rate). The ciphertext information $s(t)$ transmitted in channels are displayed in Fig. 17. Obviously, even if the transmitted signal is eavesdropped, the third party can not extract the real useful message signals.

Figure 18 demonstrates the identification process of $\boldsymbol{A}$, which conceals the message signals. They are in accordance with theoretical analysis ($\boldsymbol{D}^{-1}(\boldsymbol{A}-\boldsymbol{B}_{\mathrm{ref}})$).

From Eq. (14), we have

$$\begin{aligned}&(x_2-x_1)(a_1-b_1)\to 0,\\&x_1(a_2-b_2)-x_2(a_3-b_3)\to 0,\\&-x_3(a_4-b_4)\to 0.\end{aligned}$$

Because the complex function set $\{x_2-x_1\}$ is complex lin-

early independent, according to CLI, the corresponding $a_1 \to b_1$. Similarly, as $\{x_1, -x_2\}$ is complex linearly independent, $a_2 \to b_2$, $a_3 \to b_3$. Since $\{-x_3\}$ is complex linearly independent, $a_4 \to b_4$. The above simulations display that the outcomes are in agreement with the above theoretical analysis.

5. Conclusions

We have proposed an acoustic communication scheme based on complex parameter modulation and a complex Lorenz system for underwater wireless communication network. Firstly, we design a feedback controller and parameter updates laws in complex-variable form with rigorous mathematical proofs, while many previous references on real-variable form were only special cases in which the imaginary part was zero. Secondly, we design a novel secure communication scheme based on complex parameter modulation and the complex Lorenz system as the parameter space of the complex Lorenz system is large enough. We also find that there exist parametric attractors in the complex Lorenz system. Finally, we make simulations with the case of two-parameter modulation for digital signals, and verify the effectiveness of our proposed schemes.

References

[1] Yang G 2012 *Research on Key Security Technology of Underwater Wireless Communication Networks* (Ph.D. Dissertation) (Qingdao: Ocean University of China) (in Chinese)

[2] Syed A and Heidemann J 2016 *Time Synchronization for High Latency Acoustic Networks* April 10–15, 2016, San Francisco, CA, USA, p. 161

[3] Hu F, Malkawi Y, Kumar S and Xiao Y 2008 *Wirel. Commun. Mob. Comput.* **8** 1165

[4] Castelluccia C, Chan A and Mykletun E 2009 *ACM Trans. Sensor Network.* **5** 1

[5] Proakis J, Sozer E, Rice J and Stojanovic M 2001 *IEEE Commun. Mag.* **39** 114

[6] Wang X, Wang Y, Wang S, Zhang Y and Wu X 2018 *Chin. Phys. B* **27** 110502

[7] Shi Q, Huang X, Yuan F and Li Y 2021 *Chin. Phys. B* **30** 020507

[8] Li C, Thio W, Sprott J, Zhang R and Lu T 2017 *Chin. Phys. B* **26** 120501

[9] Wang X, Wang Y, Wang S, Zhang Y and Wu X 2018 *Chin. Phys. B* **27** 110502

[10] Li X, Chao W, Yang Z, Lei Y and Song H 2018 *Digit. Signal Process.* **81** 129

[11] Chen M, Xu W, Wang D and Wang L 2019 *IET Commun.* **13** 2097

[12] Fowler A and Gibbon J 1982 *Physica D* **4** 139

[13] Gibbon J and McGuinnes M 1982 *Physica D* **5** 108

[14] Zhang F 2015 *Entropy* **17** 4974

[15] Liu J, Wang Z, Shu M, Zhang F, Leng S and Sun X 2019 *Complexity* **10** 7242791

[16] Guo J, Ma C, Wang Z and Zhang F 2020 *Entropy* **22** 1260

[17] Huang D 2005 *Phys. Rev. E* **71** 037203

[18] Lin W 2008 *Phys. Lett. A* **372** 3195

[19] Zhang F, Sun K, Chen Y, Zhang H and Jiang C 2019 *Nonlin. Dynam.* **95** 3161

[20] Zhang F, Li M, Leng S and Liu J 2019 *J. Qilu Univ. Technol.* **33** 70

[21] Liu J and Liu S 2017 *Appl. Math. Model.* **48** 440

[22] Liu J, Chen G and Zhao X 2021 *Fractals* **29** 2150081

[23] Li C, Lei T, Wang X and Chen G 2020 *Chaos* **30** 063124